Hailfalls and Hailstorm Feeder Clouds—an Alberta Case Study

LAWRENCE CHENG

Resource Technologies Department, Alberta Research Council, Edmonton, Alberta, Canada

DAVID C. ROGERS

Department of Atmospheric Science, Colorado State University, Fort Collins, Colorado

(Manuscript received 28 July 1987, in final form 22 April 1988)

ABSTRACT

Observational evidence from an Alberta hailstorm was examined in an attempt to demonstrate the link between feeder clouds and hailfalls. Radar data, time resolved surface collections of hail, and cloud photographs from a storm were analyzed. It was found that the streak events in the surface hailfall can be linked to small-scale radar reflectivity maxima in the new growth region of the storm. The results suggest that the hail growth process began with packets of hail embryos in distinct feeder clouds, and that the separation between feeder clouds was eventually manifested as distinct hail streak events at the surface. The feeder clouds formed approximately in a line parallel to the vertical ambient wind shear near the cloud base level. The spacings between feeder clouds were almost equal and estimated to be 3 km. Theoretical predictions indicate that convective spacing in a horizontally uniform atmosphere is determined by environmental wind shear, stability, and depth of the shear layer. The results of this and other observational studies lead to the speculation that the spacing between distinct hail streak events may be controlled by the same factors in the vicinity of the new growth zone of hailstorms.

1. Introduction

The mechanisms of hailstone growth in clouds have been a topic of considerable scientific interest for many years (Schumann 1938; Ludlam 1958; Browning 1963; Foote and Knight 1977; Heymsfield et al. 1980). A problem of paramount importance in understanding hail production is the mechanism by which a hailstone embryo can be maintained in a region of adequate liquid water content long enough to grow to a hailstone. In consideration of the hydrometeor growth processes and the environment for hailstone formation, Marshall and Hitschfeld (1973) proposed a two-stage hail growth. The first stage produces hydrometeors (hailstone embryos) only as far as raindrops, or more likely as graupel and aggregates in high number density. The growth is not necessarily in the updraft of the main storm, but possibly elsewhere (Foote 1985). Large hail develops in the second stage, where a limited number of the hail embryos of the first stage find their way into the strong storm main updraft. The updraft provides suitable length of time, cold temperature and high liquid water content in which the hail embryos can grow rapidly to hail.

Barge and Bergwall (1976) studied the general characteristics of fine-scale radar reflectivity patterns of Alberta hailstorms and inferred that hailstone embryos are initiated within small updrafts of shelf clouds in the new growth region. Heymsfield et al. (1980) and Heymsfield and Musil (1982) investigated the hail growth mechanism with dual-wavelength radar data, three-dimensional tri-Doppler synthesized wind field data, in situ aircraft measurements and particle trajectory calculations within a multicellular hailstorm in northeast Colorado. They also suggested the two-stage hail growth model in which hail embryos originate in cumulus congestus adjacent to a hailstorm (feeder cells) and are advected into the main updraft region where they continue to grow. Krauss and Marwitz (1984) studied the microphysical characteristics in feeder clouds adjacent to the main updraft of a supercell hailstorm in Alberta. They showed that the feeder clouds provided a viable source of hailstone embryos and presented a vital link among hail formation processes within a broader-scale continuum of hailstorm structures. However, no direct evidence or relationship has been established between storm hailfall and feeder clouds.

The feeder cloud represents an unstable convective element located at the inflow region upwind of the main storm updraft (Dennis et al. 1970). It first forms as a small cumulus cloud (turret) with tops between 3 and 7 km and is usually located at the right flank of the storm motion. The feeder clouds frequently appear in lines and stairstep arrangement extending from the vi-

Corresponding author address: Alberta Research Council, P.O. Box 8330, Postal Station F, Edmonton, Alberta, Canada T6H 5X2.

sual edge of the main storm to appreciable distances from the hailstorm core. During their 20 to 30 minute lifetime, feeder clouds approach and finally merge with the main storm (Lemon 1976). Thus, precipitation-size particles which originate in feeder clouds may become hailstone embryos when they entrain into the main updraft. Feeder clouds form quasi-periodically in the same relative location and may determine the evolution of the storm (Fankhauser et al. 1982). The mechanism for their quasi-periodic formation is not yet known.

In this study the radar reflectivity pattern and surface observations of hailfall from an Alberta storm are examined to investigate the link between feeder clouds and hailfalls. The storm and its environment are described in section 2. The radar echo structure at low elevation scans are examined in section 3. The variations of hailfalls deduced from time-resolved hailstone samples are discussed in section 4. Trajectories of small-scale radar reflectivity patterns are presented in section 5. Echo structure in the new growth region of the storm is examined in section 6. Discussion on a speculative mechanism for the quasi-periodic development of the feeder clouds will be presented in section 7, and a summary will appear in section 8.

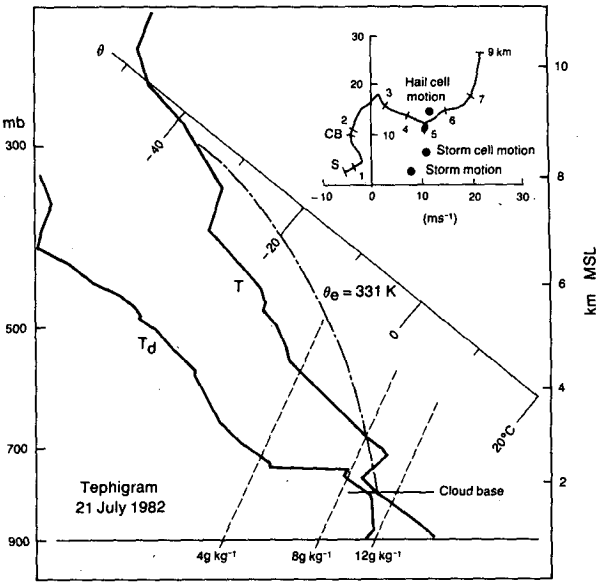

FIG. 1. Environmental sounding at 1800 MDT 21 July 1982 at Penhold, Alberta. The radar storm motion, mean storm cell motion and mean hail cell motion are also shown in the hodograph.

2. General description of the storm and its environment

On 21 July 1982, a major storm developed around 1400 (all times local mountain daylight times, MDT) just west of Rocky Mountain House in the foothills of central Alberta and tracked east-northeast, leaving a broad swath of golfball-size and larger hail (3.3–5.2 cm diameter). The storm lasted more than 7 hours and eventually moved out of radar range. The Alberta Research Council S-band meteorological radar (Humphries and Barge 1979) measured maximum reflectivities above 70 dBZ. In this paper, the word "reflectivity" is used for "equivalent radar reflectivity factor".

The representative environmental sounding and hodograph for the storm are shown in Fig. 1. The sounding was taken at 1800 in Penhold (QF) about 40 km southeast of the storm. The estimated condition at cloud base (temperature 11°C and mixing ratio 10.2 g kg^{-1}) are indicated. The cloud base temperature and pressure observed by the research aircraft at 2100 was 9.4°C and 797 mb. Below cloud base the environment was slightly unstable. A 500 m thick inversion layer was located slightly above cloud base; cloud base air parcels were negatively buoyant by 1.5 °C at the inversion. The convective available buoyant energy and the bulk Richardson number (Weisman and Klemp 1982) are estimated to be 877 $m^2 s^{-2}$ and 11.

Strong environmental wind shear above and below the level of cloud base is shown in the hodograph. The magnitude and direction of the vertical shear in the layer above cloud base, from 2 to 3 km MSL, was estimated to be $\sim 1.0 \times 10^{-2}$ s^{-1} and 25°. This strong shear layer was very stable (cf. Fig. 1). The average storm motion was approximately 8 m s^{-1} from 250° significantly to the right of the mean upper-level wind.

3. Radar echo structure at low elevation scans

Radar reflectivity patterns have commonly been used to distinguish storm characteristics. For example, Marwitz (1972) classified storms according to reflectivity pattern, evolution and wind shear. Local maxima of large-scale features in the reflectivity field as seen on PPIs have been used by Chalon et al. (1976) and Foote and Wade (1982) to study the cellular structure and evolution of multicellular storms in northeastern Colorado. Using a zenith pointing Doppler radar, Battan (1975) showed that a series of small-scale updraft cores, which were separated by regions of weak updrafts or downdrafts, existed in a hailstorm. For the most part, the highest reflectivities were outside the updraft cores. Barge and Bergwall (1976) examined the local maxima of reflectivities represented by closed contours or protrusions from large scale patterns to delineate the hail growth mechanisms in Alberta storms. They consistently found these fine scale radar reflectivity patterns in various types of storms, e.g., supercellular and multicellular, and suggested that the fine-scale patterns may well represent an important scale which must be considered in hail growth.

For the 21 July 1982 storm, the period 1800 to 1820 was studied intensively since surface hailfall observations were made at that time. This section of the paper emphasizes the small-scale radar reflectivity maxima, which are similar to those described in Barge and Bergwall.

The low-altitude structure and motion of this storm from 1758 to 1822 are shown by 0.8° elevation PPIs (approximately 0.6 km above ground at the storm location) in Fig. 2. The storm had multicellular structure and was similar to the severe Alberta hailstorm studied by Marwitz and Berry (1971). Storm cells within the storm tracked significantly to the right of the mean tropospheric winds, but to the left of the mean storm motion, as indicated on the hodograph in Fig. 1. Note that a new storm cell developed to the south during the end of the storm at 1758. The cell reached its maturity at 1807 with maximum reflectivity exceeding 65 dBZ. The mature stage of this cell lasted more than 15 min and started to decay after 1822. At this time a new storm, with reflectivity above 45 dbZ at 0.8° PPI, formed 25 km to the southwest of the storm studied. The two storms eventually merged at a later time.

Figure 3 shows the detailed structure of this storm cell at 1807 to 1822. The storm cell consisted of, and was maintained by, a number of smaller cells or local reflectivity maxima. Since radar reflectivity is an integral measure of the size and concentration of hydrometeors, a radar local reflectivity maximum represents a distinct packet of precipitation size particles. These local maxima will be referred to as hail cells. Smaller scale structure cannot be resolved with the existing radar data since the sample volume at this location is about 1 km^3. New hail cells formed at the south end of the storm cell studied and tracked approximately along the midlevel winds. Their mean motion is also shown on the hodograph in Fig. 1. Hail cells C_1, C_2 and C_3 are associated with hailfall observations at the surface and were therefore examined in detail. The C_1 cell passed its maximum at or before 1807 and dissipated thereafter. The C_2 cell first appeared in the 0.8° PPI at 1807 and reached its maximum at about 1813. The C_3 cell appeared to the south–southwest of C_2 and attained its maximum at about 1816.

4. Temporal variations of hailfalls

Time-resolved hailstone samples were collected from the storm cell discussed above. The sampling and measuring techniques have been described in Cheng and English (1983) and Cheng et al. (1985). Three storm-chase vehicles were directed underneath the high-reflectivity zones of the hailstorm. Because of the movement of storm and road constraints, the number of hailstone samples collected and the number of sampling locations were rather limited. At one of the sampling locations, hailfalls were observed for about 8 minutes (1812–1820). This sampling location (accuracy 0.8 km) is identified as a dot in Fig. 2 and as a solid square in Fig. 3. Unfortunately, the total sampling period did not cover the whole hailfall duration at this location. The sampling log and the lowest elevation radar scan above the sampling site (Figs. 2 and 3) indicate that hail might have started about 5 minutes prior to sampling.

The sampling duration for individual hail samples was short, varying from 15 to 30 seconds. A total of 19 samples was collected. The number of hailstones in a sample varied from 12 to 798. Among the 19 samples, 15 samples contained more than 100 stones and 12 samples had more than 200 stones. The time variations of the integral hail parameters calculated from the sizes and concentrations of the hailstone samples are shown in Fig. 4a. The total hail number concentration (N_T), hail water content (W_H) and hail kinetic energy (KE) are presented. Hailstones were assumed to have a density of 0.9 g cm^{-3} and fall at terminal velocity. These integral hail parameters varied considerably with time: values fluctuated more than an order of magnitude, with an extreme of four orders of magnitude in the total hail kinetic energy.

Hailstones fell onto a 1 m^2 aperture conical mosquito netting and were directed into collection bottles through a 10 cm diameter flexible hose. Some variations from sample to sample might have been caused by human reaction time and the surface friction of the sampling system. To minimize the effect of these factors, the analysis combined samples into one minute intervals. The N_T, W_H and KE calculated from one-minute accumulated samples are shown in Fig. 4b. Note that most of the high frequency fluctuations in Fig. 4a have been removed. There appears to be two distinct hailfall events separated by the minimum at 1814:30. This minimum corresponds to the radar reflectivity col between C_2 and C_3. Taking into account the trajectory of the hail cells, the accuracy of sampling location, and some delay to allow for the hail to fall, the hailstones collected before 1814:30 seem to be from C_2, and those after 1814:30, from C_3.

Distinct hail cells have been identified in time-resolved surface hail collection elsewhere. Federer and Waldvogel (1975) used an automatic hail spectrometer to study the hailstone size frequency distribution from a Swiss multicell storm. The sampling interval of the instrument was 30 seconds. The hail spectra were obtained from the most vigorous cell of the storm which produced a number of hailswaths. Their data showed that during a 14-minute sampling period, four different hail cells, each one lasting approximately 2 to 3 minutes produced the hailswath. The storm motion and storm cell motion of the Swiss storm were slower than our Alberta storm.

Figure 4c shows the time variation of the maximum hailstone equivalent volume diameter (D_{max}) and equivalent radar reflectivity factor (Z) calculated from the sizes and concentrations of the hailstone samples using the back-scattering amplitude for wet hailstones (non-Rayleigh particles with 0.05 mm water thickness) at a frequency of 2.88 GHz. The 1-minute averages are also included. The calculated radar reflectivity factor varied from 38 to 61 dBZ. Radar reflectivities over the sampling location were taken from the PPIs in Fig. 3 and plotted in Fig. 4c for comparison. The agreement

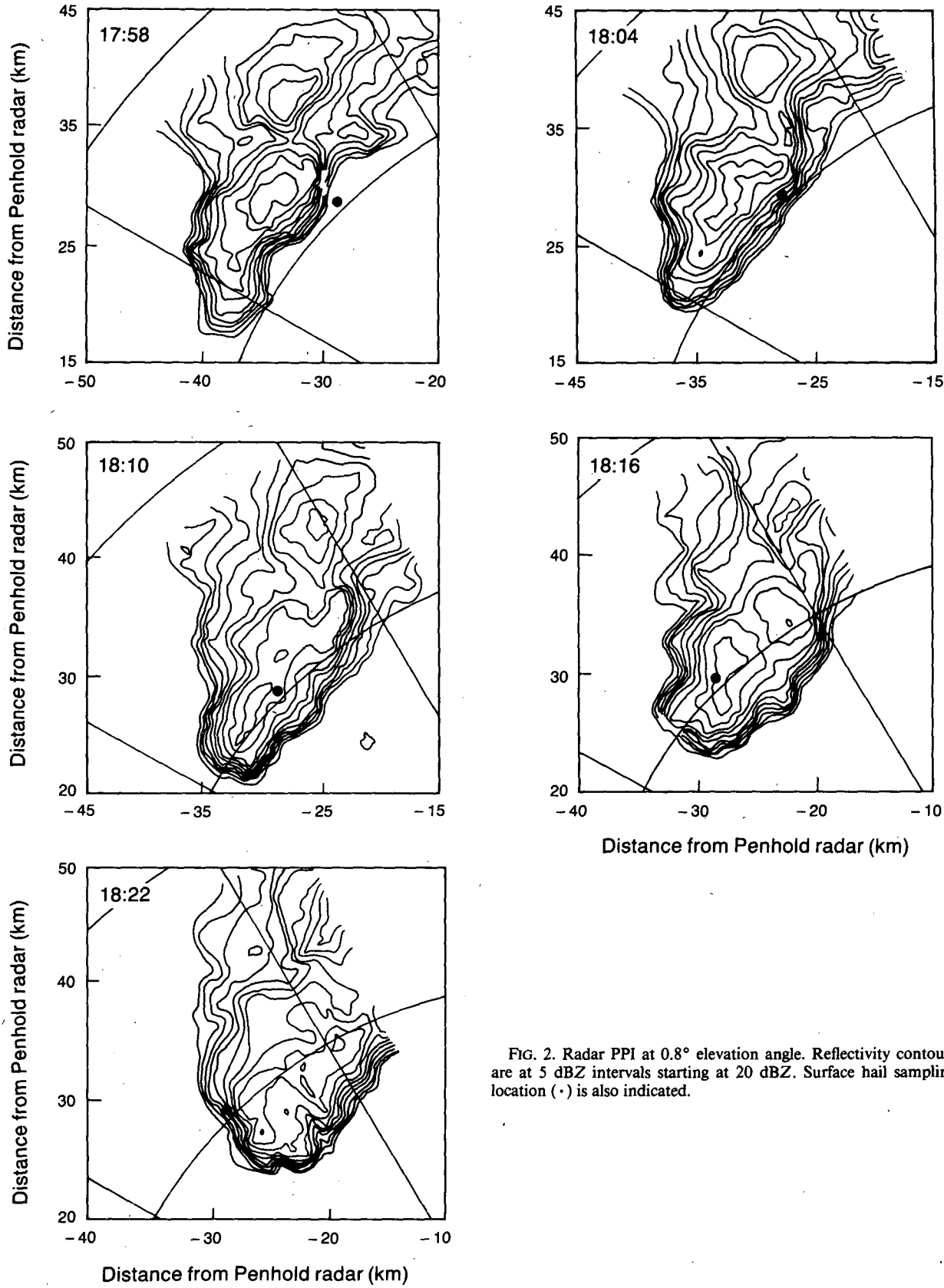

FIG. 2. Radar PPI at 0.8° elevation angle. Reflectivity contours are at 5 dBZ intervals starting at 20 dBZ. Surface hail sampling location (·) is also indicated.

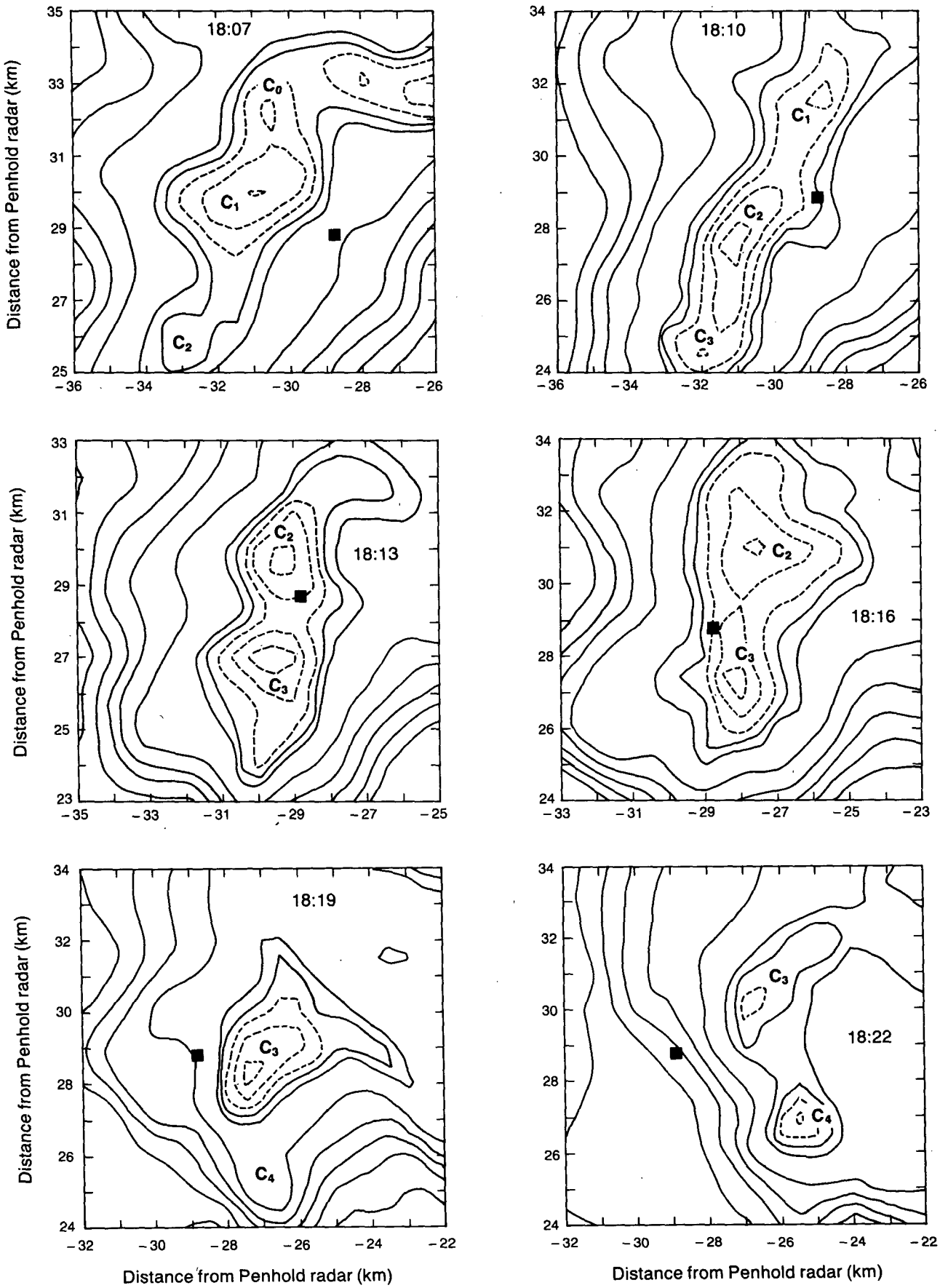

FIG. 3. Limited area display of 0.8° elevation scan radar PPI at 1807 to 1822 MDT. Solid reflectivity contours are 10, 20, 30, 40, 50, 60 and 62 dBZ, and dashed contours 64, 66 and 68 dBZ. The solid square indicates the surface sampling location.

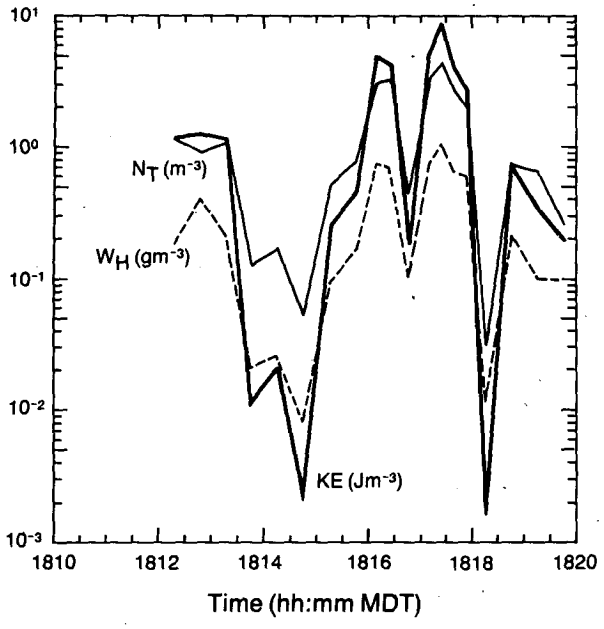

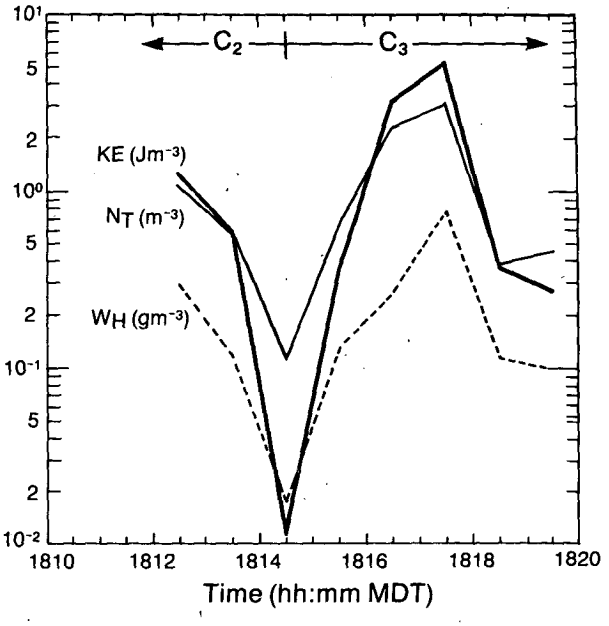

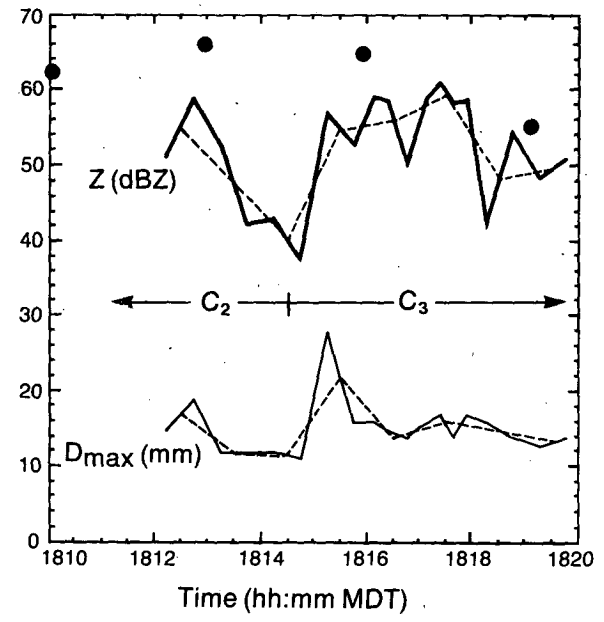

FIG. 4. Hail parameters obtained from surface hailstone samples obtained at the location shown in Figs. 2 and 3. (a) Total hail number concentration, N_T, hail water content, W_H, and hail kinetic energy, KE; (b) 1-minute values of N_T, W_H and KE; (c) raw (solid line) and 1-minute values (dashed line) of radar reflectivity factor, Z, and maximum equivalent volume diameter, D_{max}.

between observed and calculated reflectivities is probably about as good as could be expected, given the large differences in sample volume and resolution of radar and surface sampling. The radar reflectivities were approximately 8 dBZ larger than calculated surface values, which is consistent with the possible melting of hailstones below 0°C. The 1-minute values of Z and D_{max} are consistent with N_T, W_H and KE, which show an apparent reduction of hailfall at 1814:30. The peak of D_{max} just after 1814:30 may be attributed to the size sorting process described by Auer and Marwitz (1972): the largest hailstones reach the ground first. This idea is consistent with the assumption that there were two distinct hail packets.

5. Evolution and trajectories of small-scale radar reflectivity patterns

The radar data measured during the hailstone sampling period and close to the sampling location were examined carefully to look for small-scale patterns. In this study, the small-scale radar reflectivity patterns are determined from the digital radar bin arrays; in contrast, Barge and Bergwall (1976) and Krauss and Mar-

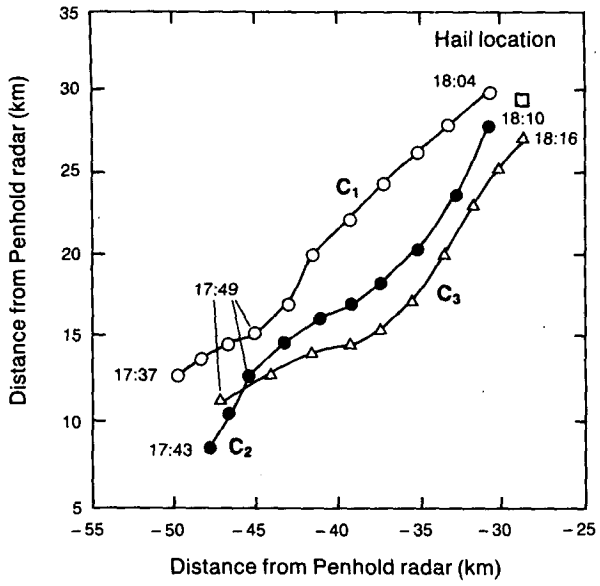

FIG. 5. Horizontal trajectories of the center (local maximum) of the small-scale reflectivity patterns; C_1, C_2 and C_3. The start and end times of each trajectory are shown, together with cell center locations every 3 minutes (time between radar scans).

witz (1984) used computer-generated contours. The evolution of the small-scale radar patterns (hail cells) C_1, C_2 and C_3 are discussed below.

A number of criteria were established to ensure that the small-scale radar reflectivity pattern represents a distinct packet or entity of hydrometeors:

(i) The packet is persistent in space and time.
(ii) Its reflectivity value increases with time except when warmer than 0°C.
(iii) The packet moves in the general direction of the midlevel wind.
(iv) The packet must move downward if its maximum value is larger than 60 dBZ.

The first criterion asserts the continuous nature of the reflectivity entity. The second criterion is for choosing the hydrometeor packets which are growing toward hail stage; melting would reduce the radar reflectivity value of the packet. The third criterion provides a probable estimate of the hydrometeor horizontal trajectory. The 60 dBZ criterion assures the existence of hail, which should fall out of the storm.

The hail cells C_1, C_2 and C_3 were tracked backward in time and space using the above criteria. The horizontal trajectories of the centers (maxima) of these small-scale radar patterns, which were derived by projecting the maximum reflectivities at any height onto a horizontal surface, are shown in Fig. 5. The results indicate that these packets originated at about the same region of the storm and their horizontal trajectories were very similar. Figure 6 shows the trajectories of

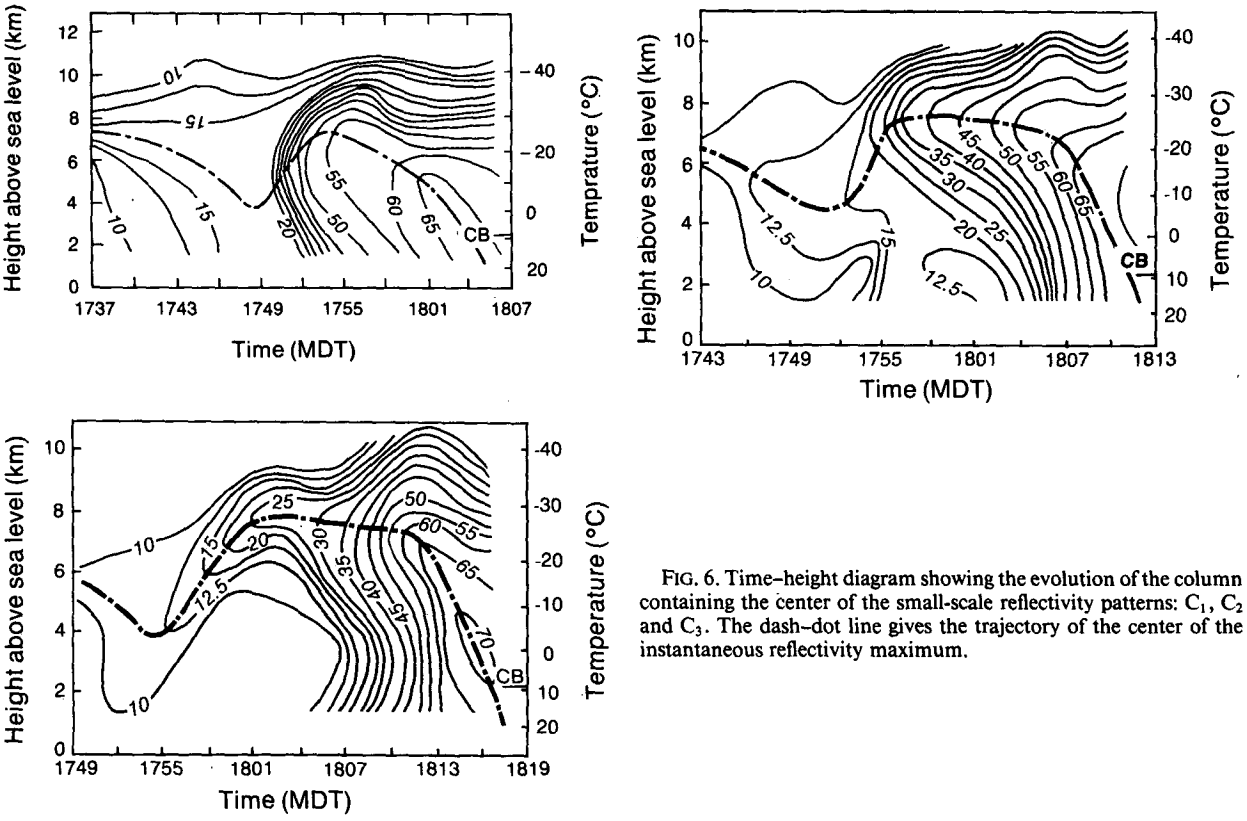

FIG. 6. Time–height diagram showing the evolution of the column containing the center of the small-scale reflectivity patterns: C_1, C_2 and C_3. The dash–dot line gives the trajectory of the center of the instantaneous reflectivity maximum.

the centers and the evolutions of the small-scale radar patterns in time–height section. The figures were constructed by plotting the column of reflectivity containing the small-scale maximum for each time. The evolutions and trajectories of the center of these packets are similar. The trajectories lasted approximately 30 minutes, from the first radar echo (exceeding the radar detection limited) until the center descended to the ground. First radar echoes were found at about −15° to −20°C level. For the first 10 minutes or so, the packets fell, and their reflectivity values slowly increased. Then a period of rapid ascent (~15 m s^{-1}) and hydrometeor growth (~4 dBZ min^{-1}) followed. The maximum vertical velocity of the storm calculated from the environment sounding using the loaded moist-adiabatic (LMA) cloud model developed by Chisholm (1973) was 33.5 m s^{-1}. The growth from 25 to 60 dBZ (probably hail) occurred within 10 to 12 minutes at about −25°C. This is similar to the temperature range of hailstone growth deduced by Knight et al. (1981) and Federer et al. (1982) using isotopic analysis, and by Nelson (1983) and Foote (1984) who used a combination of Doppler radar synthesized winds and numerical hail growth models. The long growth period and the moderate updraft derived from the radar reflectivity maxima are consistent with the results of Nelson (1983)—that large hail growth occurs in a broad region of moderate updraft (20–40 m s^{-1}). Growth continued as the packets fell. The center of packet C_2 hit the ground at about 1811 and C_3 arrived at about 1817. These extrapolated fallout times when the packets reached the ground near the sampling location are consistent with the surface hailfall observations.

6. Echo structure in the new growth region

The data presented so far suggest that the new growth zone is probably a "breeding ground" for hailstone embryos, and therefore deserves special attention. Radar PPIs in the new growth region of the storm were examined, beginning 23 minutes before the first hail sample and continuing through the sampling period. Figure 7a shows the 1.8° PPI (about 1.5 km AGL, or 400 m above cloud base) at 1749, and Fig. 7b is the vertical cross section extending from the storm center through the line of feeder clouds. As mentioned earlier, the distinct maxima C_1, C_2 and C_3 were identified by tracking them backwards in time from where they were quite obvious (Fig. 3). At 1749, the reflectivities in these cells were small, and the tracking analysis used the digital radar bin arrays. It is instructive to compare the vertical cross section in Fig. 7b with the time–height histories of these cells. At 1749 in Fig. 6a, C_1 was at a relatively low altitude and about to begin a period of rapid ascent and rapid increase in reflectivity. This corresponds to C_1 moving up and to the right, along the top of the weak echo region in Fig. 7b. This description is consistent with the current concepts of hail growth trajectories (Nelson 1983; Foote 1984). If we conjecture that C_2 and C_3 followed paths similar to C_1, then the formation of discrete packets of hail is suggested in Fig. 7b; C_2 is the next emerging packet of embryos, and after it, C_3, which has just become radar detectable. Packet C_2 will arrive at the low point of C_1 in about 3 minutes (cf., Fig. 6b), and C_3 will arrive about 3 minutes later.

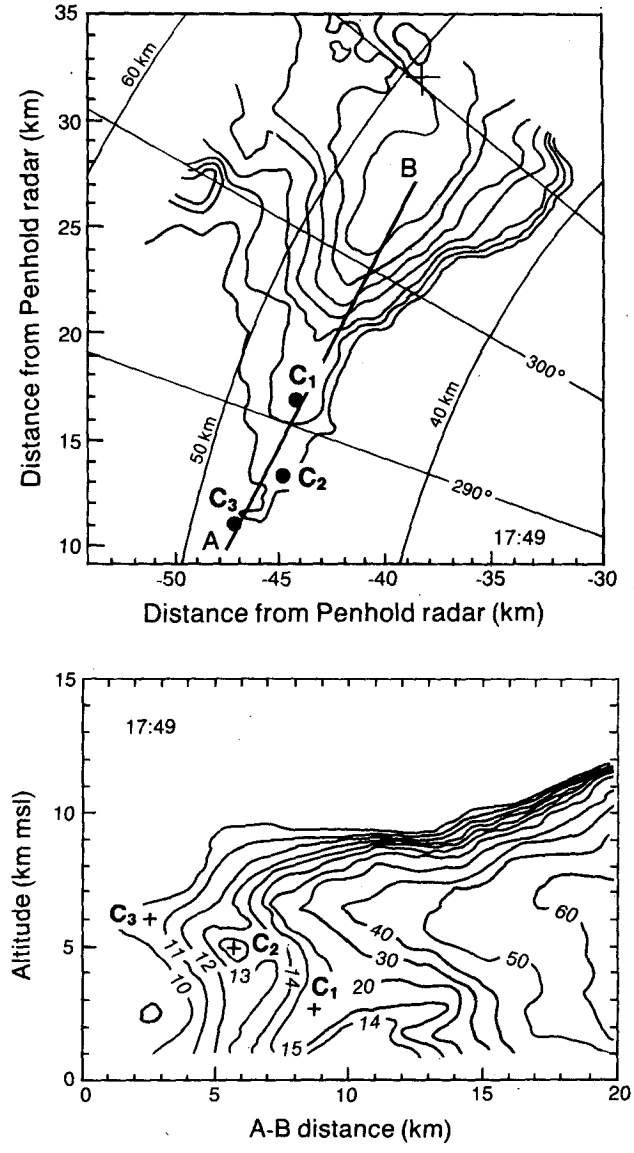

FIG. 7. (a) Radar PPI at 1.8° elevation angle through the new growth region of the 21 July 1982 storm. The horizontal locations of small-scale reflectivity maxima C_1, C_2 and C_3 (projected onto the PPI) are shown by dots. Reflectivity contours are 10, 15, 20, 30, 40, 50 and 60 dBZ. (b) Radar vertical section along line AB. The fiducial plus (+) marks give the locations of local reflectivity maxima C_1, C_2 and C_3.

This kind of sequence was not an isolated event in the storm. For example, another 1.8° PPI is shown in

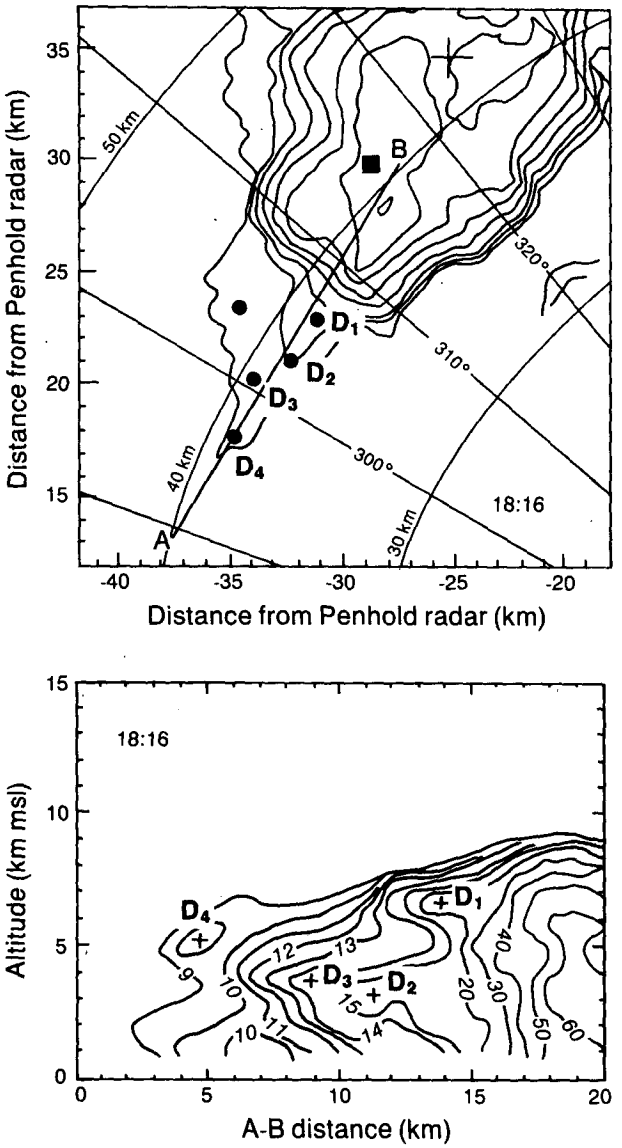

FIG. 8. As in Fig. 7 but for 1816 MDT. The hailstone sampling location (1812 to 1820) is denoted by the solid square.

Fig. 8a at 1816, when the surface hailfall observations were made. Figure 8b is the corresponding vertical cross section along the feeder cloud line. Distinct small scale maxima D_1, D_2, D_3 and D_4 were identified the same way as in the C series: by tracking maxima backwards in time from when they were quite obvious (see Fig. 9). The horizontal and vertical trajectories of these packets are shown in Fig. 10. The packets moved with the same general direction and speed as the C series. The vertical trajectories possessed the same down–up–down characteristics. Horizontal spacings between these packets were rather uniform, about 3 km (similar to the C series also). The first radar echos were also found at about −15 to −20°C. Notable differences between the later two packets (D_3 and D_4) and the earlier two packets (D_1 and D_2) in this series are that the duration or lifetime of these packets was shorter, and their trajectories were somewhat lower. The maximum reflectivities of D_3 and D_4 were approximately 50 dBZ, whereas D_1 and D_2 were 60 dBZ. This suggests that hydrometeor growth in D_3 and D_4 was not as strong. At their trajectory end points, they were almost located within packet D_2. Packets D_3 and D_4 could have been affected by the particles falling from the anvil of a storm to southwest. Fig. 11 is the 6.9° PPI (about 5 km above ground) at 1819. Note that the 10 dBZ contour shows the two storms almost linked together.

The line of feeder clouds in the new growth zone was evident as a low reflectivity protrusion and persisted at the same relative location with respect to the storm for the entire 33-minute analysis period. The spacings between these radar reflectivity maxima are summarized in Table 1. The mean distance between the maxima along the environmental wind shear ranges from 2.4 to 3.3 km (and could be nearly constant, considering the resolution of the data, 0.7 km). A line joining the maxima is approximately parallel the environmental wind shear vector near cloud base level (25°, cf., Fig. 1). This line started to curve at 1822, as shown in Fig. 12, when the nearby storm moved close to the storm studied; they eventually merged at a later time. This change in orientation of the feeder line illustrates the importance of environmental influences on storm structure and evolution.

Cloud photographs also provided some information about feeder cloud spacing. The photographs were

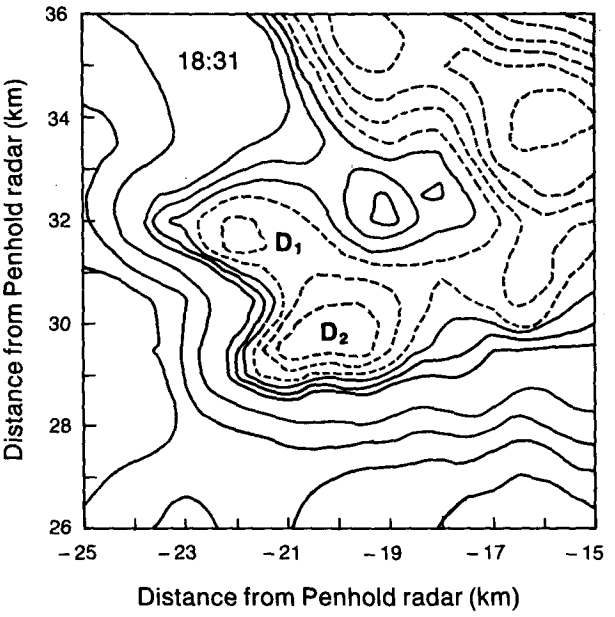

FIG. 9. Limited area display of 0.8° elevation scan radar PPI at 1831 showing the end points of the trajectories for packets D_1 and D_2. Solid reflectivity contours are 10, 20, 30, 40, 50, 52 and 54 dBZ, and dashed contours 56, 58, 60, 62 and 64 dBZ.

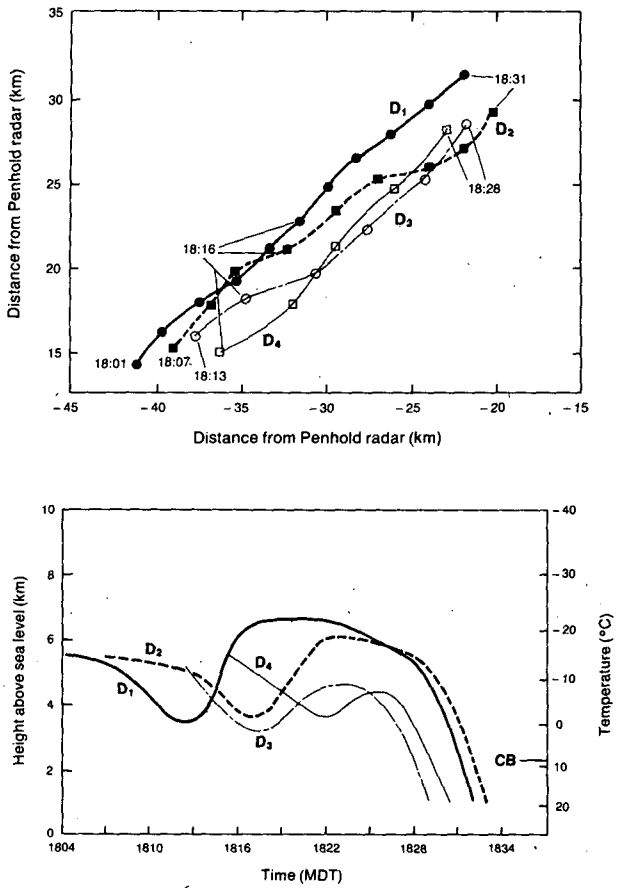

FIG. 10. Horizontal (a) and vertical (b) trajectories for packets D_1, D_2, D_3 and D_4. Symbols are located at 3-minute intervals, and the start and end times of each horizontal trajectory are given. Locations of the packets at the time of Fig. 8 (1816) are also indicated.

taken during a research flight about two hours after the hailstone samples were collected at the ground. Although thunderstorms can undergo a significant evolution in two hours, the cloud features in the picture provide additional information about feeder cloud spacing. Figure 13 shows a picture of the new growth region taken at 2113; three feeder clouds with intense growth are apparent. The photograph was taken from the research aircraft looking northeast toward the new growth region. The feeder clouds were located at the southwest corner of the storm, similar to those shown in Figs. 7 and 8. The reflectivity maximum of the storm at this time exceeded 65 dBZ, and hail larger than golfball size was reported. From the radar echo-top height and the orientation of the feeder line, the average spacing between these cloud turrets was estimated to be 3 km. Unfortunately, the storm was located about 90 km from the radar site at this time, and the radar minimum detectable signal at this range is 17 dBZ, with spatial resolution 1.6 km. Therefore, a study of the reflectivity pattern in the storm's new growth region was not possible, and a direct comparison between the cloud picture and the radar reflectivity pattern at this time could not be made. Nevertheless, the spacings between the feeder clouds obtained from the cloud picture are similar to those two hours earlier.

The spacing between cloud turrets and the episodic (or periodic) events associated with the hailfalls at the surface seem to be connected by a cause and effect relationship. The available evidence suggests that packets of particles (probably hail embryos) that were initiated within the updrafts of feeder clouds in the new growth region were transported by the wind field and entered the main updraft region where they grew rapidly to hail size. These packets maintained distinct identities throughout their evolution in the main storm and then fell to the ground as separate entities. This is consistent with the suggestions of Heymsfield et al. (1980) and Krauss and Marwitz (1984) and is similar to the cause and effect relationship between periodic cellular evolution and low level streaks in reflectivity maxima advanced by Chalon et al. (1976).

7. Speculative mechanism for the formation of feeder clouds

Previous studies have shown that for many thunderstorms, the subcloud inflow and outflow structure can produce successive cells and affect storm propagation. Ellrod and Marwitz (1976) showed from aircraft observations that the horizontal velocity of the low-level airflow decreased sharply in the vicinity of the gust front and produced strong convergence. They found that the updraft field near cloud base was elon-

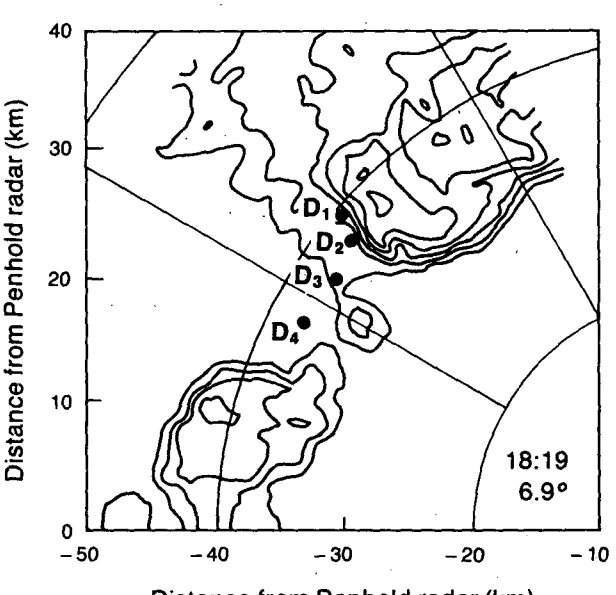

FIG. 11. Radar PPI at 6.9° of the 21 July 1982 storm, 1819 MDT. Reflectivity contours are at 10 dBZ intervals starting from 20 dBZ. Locations of small-scale reflectivity patterns, D_1, D_2, D_3 and D_4 are also indicated.

TABLE 1. Mean spacings between local reflectivity maxima in the new growth region of the 21 July 1982 storm.

Time (MDT)	Along feeder line (km)
1749	2.9
1752	2.5
1755	3.3
1758	2.4
1801	2.7
1804	2.4
1807	2.6
1810	2.4
1813	2.6
1816	3.2
1819	2.4
Mean	2.6
Std. dev.	0.3

gated and tended to be parallel to the gust front. The strongest updraft at cloud base was generally above and to the rear of the wind-shift line at or near the surface. It appeared that the updraft was enhanced by lifting of the subcloud air above the cold air outflow. Similar observations were also reported by Fankhauser (1982) from surface, radar and flight data. Furthermore, he showed that the zone of maximum surface convergence is the most favorable region for the development of new cells. In related work, Gurka (1976) found a linear relation between the average speed of cloud arcs detected by satellite and the maximum wind gust observed around thunderstorms. The development of new cells, which occur over or just behind the cold outflow boundary set up by previous cells, were also numerically simulated by Wilhelmson and Chen (1982). The persistent location of the new growth area may be the result of interactions between the inflow and outflow of the parent storm.

In the storm discussed here, feeder clouds developed along a line approximately parallel to the environmental wind shear which is concentrated within the low level stable layer. Thus, we speculate that a Kelvin-Helmholtz type of instability may be responsible for the initiation and maintenance of the periodical features of the line of feeder clouds. This periodicity would be manifested in the spacing or the recurrency rate of feeder clouds.

We thought it would be useful to pursue our speculation somewhat, by trying a simple modeling analogy. In the linear model of shear instability developed by Lalas and Einaudi (1976), horizontal wind velocities in the vicinity of the shear zone are represented by a hyperbolic tangent profile in the presence of air density that decreases exponentially with height:

$$V(z) = V_0 + V^* \tanh\left(\frac{z - z_0}{h}\right), \qquad (1)$$

where V is the horizontal wind speed along the direction of the shear vector, z the altitude above ground, z_0 the altitude of the inflection point in the vertical profile of V, V_0 the value of V at z_0, V^* is one-half the increase in V across the shear layer, and h one-half the depth of the shear layer. The Lalas and Einaudi model assumes a stratified shear flow in the atmosphere with constant Brunt-Väisälä frequency, bounded below by the ground and above by an infinite layer with constant wind and temperature. It was designed to investigate the characteristics of unstable and neutral gravity waves that can be supported in such an atmosphere. The model has been applied to the studies of wavelike rainbands (Parsons and Hobbs 1983; Wang et al. 1983)

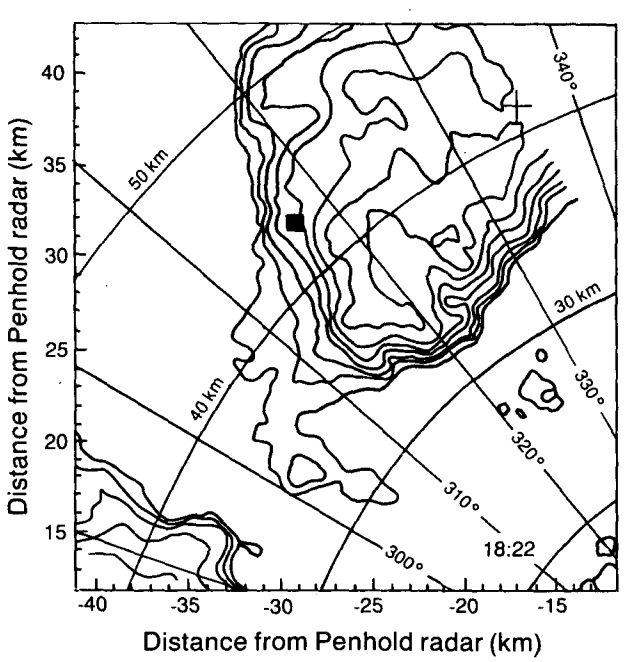

FIG. 12. Similar to Fig. 7 but for 1822 MDT. Hailstone sampling location is denoted by the solid square.

FIG. 13. Photograph taken from research aircraft at 2113 MDT looking northeast toward the new growth region. Arrows show the locations of feeder clouds.

and waves in association with the frontal shearing zone (Testud et al. 1980).

For our use, the hyperbolic-tangent profile was applied to the hodograph in Fig. 1 with the component of horizontal environmental wind along the direction of the shear layer at cloud base, and the result is shown in Fig. 14. The best-fit parameters to the sounding are: $V_0 = 10.1$ m s^{-1}, $V^* = 3.8$ m s^{-1}, $z_0 = 1265$ m and $h = 305$ m. These parameters can be used to estimate the wavelength of the shear-induced modes. According to Lalas and Einaudi, the first mode neglects the lower boundary; the other two modes are due to resonance effects from the ground. In the case studied, only the first and third modes are important because of the wind profile characteristics. The horizontal wavelengths of the unstable modes of gravity waves generated by shear flow are 2.7–4.2 and 5.8–14.2 km, with critical Richardson number 0.25 and 0.14, for mode I and mode III, respectively. The close distance from the inflexion point to the ground does not allow the existence of unstable waves for mode II. The predicted wavelength for the first mode agrees with the observed spacings between feeder clouds. From the sounding, the Richardson number in the shear layer (away from the vicinity of the storm) was 0.19, smaller than the critical value for mode I, and thus small enough to initiate the instabilities. Chimonas et al. (1980) pointed out that gravity waves generated by wind shear can attain sufficiently large amplitudes to induce condensation and that the latent heat released may reinforce the waves, i.e., gravity waves can trigger convection. This provides a possible explanation for the observed increased vigor of feeder clouds with increasing "age".

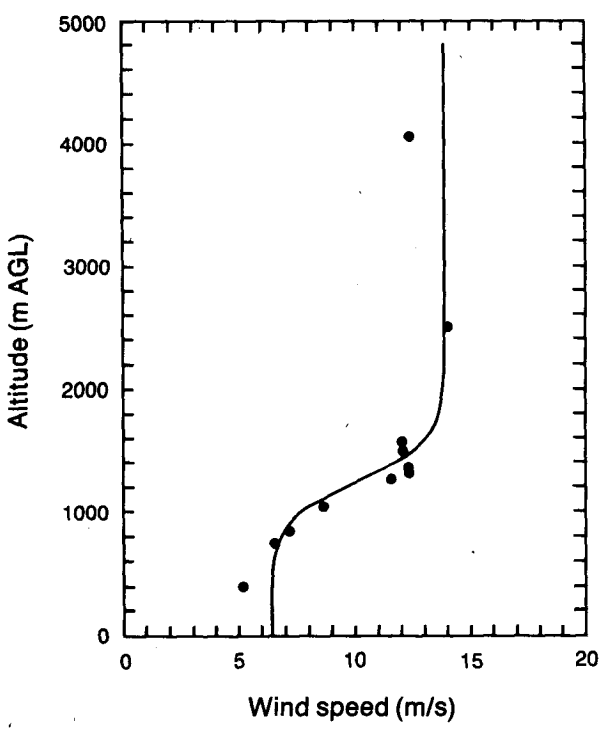

FIG. 14. Measured windspeeds (solid dots) along the vertical wind shear from the hodograph in Fig. 1. The line is the best-fit hyperbolic tangent curve to the data points.

The location of the low-level convergence due to the interaction of the storm outflow and inflow was not measured in this storm. Furthermore, the hodograph used in the above estimation was for the storm environment. Near the storm, the condition might be different, as from diffluence around the storm or its outflow. It is not obvious where the shear was most concentrated because of the three-dimensionality of the flow field. Thus, the above estimate of shear induced wavelength must be considered tentative. The speculative discussion on feeder cloud formation mechanisms is intended to stimulate additional theoretical, numerical and observational studies of the dynamic and microphysical interactions among feeder clouds, the hailstorm and the ambient environment.

8. Conclusion

A variety of observational data was presented in an attempt to find causative and controlling factors for hailstorm feeder clouds. Radar data, time-resolved surface collections of hail, and cloud photographs from an Alberta storm on 21 July 1982 were analyzed. The low elevation detailed radar scans and time-resolved surface hail data revealed separate events of hailfalls. Small-scale reflectivity patterns corresponding to hailfall events were tracked back to the new growth region of the storm. The results suggest that in the period of study for this storm, the hail growth process began with hail embryos in distinct feeder clouds. These particles were transported by the wind field and entered the main storm to continue their growth. The evidence is suggestive, though not conclusive, that the packets of hydrometeors maintained unique identities throughout their evolution in the main storm and precipitated out to the ground as distinct hail streak events.

Aspects concerning the formation mechanism of a wavelike line of feeder clouds were also examined. The persistent location of feeder clouds was speculated to be the result of interaction between the inflow and the low level outflow of the storm. The line of feeder clouds was oriented along a line approximately parallel to the environmental wind shear; this suggests that they may have been caused by a Kelvin-Helmholtz type of instability. The spacing of feeder clouds was found to be generally consistent with the resonance mode theory for shear induced instability proposed by Lalas and Einaudi (1976). Because of the influence of the storm on the mesoscale flow and on the vertical stability near the storm, the local shear instability may change in the vicinity of the storm. In cases which favor the wave propagation and amplification, a feeding line can develop. For other cases, no line of feeder clouds may form. The formation mechanism for wavelike line of